Axially loaded RC walls with cutout openings strengthened with FRCM composites

Cristian Sabau (corresponding author). E-mail: cristian.sabau@ltu.se

Ph.D. Candidate, Dept. of Civil, Environmental and Natural Resources Engineering, Luleå University of Technology, SE-971 87 Luleå, Sweden,

Cosmin Popescu

Ph.D., Northern Research Institute–NORUT, Rombaksveien E6-47, N-8517 Narvik, Norway

Gabriel Sas

Ph.D., Northern Research Institute–NORUT, Rombaksveien E6-47, N-8517 Narvik, Norway

Thomas Blanksvärd

Associate Professor, Dept. of Civil, Environmental and Natural Resources Engineering, Luleå University of Technology, SE-971 87 Luleå, Sweden.

Björn Täljsten

Professor, Dept. of Civil, Environmental and Natural Resources Engineering, Luleå University of Technology, SE-971 87 Luleå, Sweden.

Abstract

Upgrading existing buildings to new functional requirements may require new openings that can weaken the structure and prompting the need for strengthening. In such cases traditional strengthening solutions such as creating a reinforced concrete (RC) or steel frame around the opening, imply long term restrictions in the use of the structure compared to solutions that use externally bonded composites. Two fabric-reinforced cementitious matrix composites (FRCM) composites were used in this study to restore the capacity of panels with newly created door type openings to that of a solid panel. Five, half scale RC panels acting as two-way action compression members were tested to failure. Two, full-field optical deformation measurement systems were used to monitor and analyze the global structural response of each tested panel (i.e. crack pattern, failure mechanism, and displacement/strain fields). The performance of existing design methods for RC panels has been assessed in comparison with the experimental results. The capacity of strengthened panels with *small openings* (450 mm x 1050 mm) was entirely restored to that of the solid panel. However, for panels with *large openings* (900 mm x 1050 mm), only 75% of the solid panel's capacity was restored. The capacity of the strengthened panels was about 175% and 150% higher compared to that of reference panels with small and large openings, respectively.

Introduction

Upgrading existing buildings to new functional requirements may require new openings for doors, windows, or heating and ventilation systems, in existing structural elements such as reinforced concrete (RC) walls and slabs. New openings created in elements that were designed without allowances for openings are termed cutout openings. A recent literature review (Popescu et al. 2015) shows that the effect of cutout openings in structural concrete panels acting as compression members has rarely been investigated. However, available studies on the topic (Popescu et al. 2016), concluded that, cutout openings substantially decrease the load bearing capacity of solid RC panels, consequentially weakening the existing structure.

In the current social and economic climate, upgrading or retrofitting of existing buildings, is usually associated with shorter service interruptions, accessibility periods, as well as lower life-cycle costs, and is therefore often preferred to replacement with new structures (Ferreira et al. 2015; Assefa and Ambler 2017). Hence, retrofitting is, more sustainable than demolishing and rebuilding.

Traditional strengthening methods for structural walls with cutout openings involve concrete jacketing or creating a RC or steel frame around the opening. These methods usually require interventions to the building's infrastructure to extend existing foundations and can significantly contribute to the building's structural mass. The use of externally bonded composites can overcome the mentioned drawbacks. Due to their relative light weigh, their contribution to the structural mass is greatly reduced compared to traditional methods and do not require additional foundations. Recently, two epoxy-bonded fiber reinforced polymer (FRP)-based strengthening solutions for RC walls with openings subjected to axial loads have been investigated by Mohammed et al. (2013) for one way action (OW) panels and by Popescu et al. (2017a) for two way action (TW) panels. The terms OW action and TW action refer to the boundary conditions of the elements, which are restrained only on the top and bottom edges and restrained on three or four edges, respectively.

Inorganic cement-based matrices (mortars) can be used as a sustainable and durable alternative to epoxy for bonding additional reinforcement to existing RC members (Täljsten and Blanksvärd 2007; Gonzalez-Libreros et al. 2017b). The mortar matrix is reinforced with continuous fibers in the form of either a uni-directional or bi-directional net, resulting in a fabric-reinforced cementitious matrix composite (FRCM). This type of composite is also referred to as mineral-based composite (MBC), textile-reinforced mortar (TRM), and textile-reinforced concrete (TRC). The term FRCM composites will be used in this paper. The fibers commonly used in these composites include carbon, glass, and polyparaphenylene benzobisoxazole (PBO) (Sneed et al. 2014).

The effect of externally bonded FRCM composites have been extensively studied on RC beams in flexure (D'Ambrisi and Focacci 2011; Elsanadedy et al. 2013; Sneed et al. 2016), RC beams in shear (Gonzalez-Libreros et al. 2017a), and for the confinement of RC columns (Colajanni et al. 2014; Ombres and Verre 2015). In comparison, investigations on FRCM strengthening of structural walls are considerably fewer, and mostly focused on masonry panels, for example (Papanicolaou et al. 2007; Bernat et al. 2013; Babaeidarabad et al. 2014; Ismail and Ingham 2016). However, only one study that focused on the testing of RC panels with openings subjected to in-plane shear has compared the effect of a FRCM strengthening solution with that of several FRP solutions (Todut et al. 2015). It was reported that the FRCM strengthening was able to increase the capacity of damaged panels with openings to their initial capacity.

The effectiveness of FRCM strengthening of masonry members subjected to the combined effects of out-of-plane bending and axial loads (i.e., compression members) has only been investigated for masonry OW action panels (Kolsch 1998; Bernat et al. 2013; Babaeidarabad et al. 2014; Cevallos et al. 2015; Ismail and Ingham 2016). For example, Bernat et al. (2013) used FRCM composites with carbon and glass fiber nets to strengthened OW masonry panels subjected to eccentric compression. A 100% increase of the load bearing capacity of the walls was obtained. Additionally, it was concluded that for axially loaded elements, additional anchoring of the FRCM layer is unnecessary since debonding of the FRCM strengthening was not observed. Babaeidarabad et al. (2014) used carbon FRCM composites to strengthen OW masonry panels subjected to flexure. The flexural capacity of strengthened panels with one and four FRCM layers was 280% and 750% that of the reference specimen's capacity, respectively. Additionally, it was found that for the same fiber reinforcement ratio, FRCM and FRP strengthening methods provide similar increments in flexural capacity.

The topic of FRCM strengthened TW action panels or RC panels has yet to be addressed. In addition, similar studies on compression members with openings strengthened with FRCM composites have yet to be reported. Consequently, no design guidelines for strengthening of axially loaded RC walls with cutout openings using FRCM composites is available. As a first attempt, the appropriateness of existing design methods for RC panels with openings (Guan et al. 2010), to predict the capacity of FRCM strengthened panels has been assessed. However, a perfect agreement between the experimental and theoretical values is not expected since the considered model was not developed for strengthened members.

The objective of this study is to evaluate the capacity and stiffness improvements obtained by FRCM strengthening of axially loaded TW action concrete panels with openings. The FRCM strengthening solution used in this study is intended to restore the capacity and stiffness of panels, with newly created openings, to that of a solid panel. Two FRCM systems were employed with the aim of determining the influence of the composite properties on the capacity and stiffness of the strengthened panels. These systems, which were provided by different manufacturers, contain carbon fiber nets and PBO fiber nets, and are hereafter referred to as C-FRCM and PBO-FRCM, respectively.

Experimental Program

Description of Concrete-Wall Specimens

Five precast RC wall panels, each with nominal length (L), height (H), and thickness (t) of 1800, 1350, and 60 mm, respectively (Fig. 1), were considered in the test program. One was a solid panel (SW), while the other panels were each characterized by a middle section consisting of door-type openings (as illustrated in Fig. 1). Two panels had 450×1050 mm openings, referred to as *small openings* hereafter, and the other two panels had 900×1050 mm openings, referred to as *large openings* hereafter.

Furthermore, panels were designated as SO# and LO#, where SO and LO refer to the size of the opening (i.e., small opening and large opening, respectively, see Fig. 1). The # symbol denotes the FRCM system used for strengthening, and # values of 1 and 2 refer to the C-FRCM and PBO-FRCM systems, respectively (e.g., SO1 refers to a panel with a *small opening* strengthened with the C-FRCM composite). A summary of the tested specimens is presented in Table 1.

The panels were cast using self-consolidating concrete. The compressive strength of the concrete (f_c) was determined on six cubes at the day of testing (689 days) following the procedure described in EN ISO 12390-3 (2009). An average compressive strength of 68.0 MPa was obtained.

The internal reinforcement consisted of one layer of 5-mm welded steel-wire fabric. The steel reinforcement net was placed in the center of the concrete section, with the steel bars in the vertical and horizontal directions, as shown in Fig. 1. The yield strength (f_y) was determined on five coupons in accordance with EN ISO 15630-2 (2010). An average f_y of 634 MPa and mean ultimate strength f_u of 693 MPa at mean strain values of 2830 µm/m and 48690 µm/m, respectively, were obtained. The panels were stored in the vertical position in a dry environment up to the day of strengthening.

No additional reinforcement was placed around the edges or corners of the openings to replicate practical cases when sawn cut-outs are created in existing solid panels. For convenience, the panels were designed having openings instead of cutting them out from solid panels, as this choice is believed to not influence the behavior of the tested panels. However, in practical application, because the load on the panel cannot be completely removed if openings are cut-out before strengthening, the panel might suffer additional damage or deformations.

Strengthening Solution

Composite Properties

Each FRCM system consisted of a fiber net and corresponding mortar (see Table 2). The mechanical properties of the fibers, namely, the ultimate tensile strength f_f, ultimate tensile strain ε_f, and modulus of elasticity E_f, are summarized in Table 2. The geometrical properties of the net are characterized by the center-to-center bundle spacing b_f, bundle width b^*, and bundle thickness t^*. Moreover, the equivalent dry-fiber thickness t_f was taken as the value reported by the manufacturer, whereas the cross-sectional area of the bundles A_b^* was determined from the linear mass density of the bundles, as stipulated by ASTM D1577 (2007). The average values of A_b^* and t^* are listed in Table 2. A nominal composite thickness (t_{FRCM}) of 8 mm was chosen for both

FRCM systems (Fig. 1) to obtain similar FRCM reinforcement ratios $\rho_{FRCM}=t_f/t_{FRCM}$ (i.e., $\rho_{FRCM}\cong 0.57\%$), t_{FRCM} was chosen with consideration of the minimum mortar-layer thickness recommended in the product technical sheet of each system. After strengthening, the total thickness of the panels was measured in multiple locations. An average FRCM thickness of 11 mm was obtained. The carbon net had the same fiber area in both directions (i.e. balanced bi-directional net), grouped in bundles with 20 mm spacing. The PBO net had the fiber area predominantly in one direction (i.e. uni-directional net), grouped in bundles with 12 mm spacing. The PBO net also had bundles with 3 mm spacing in the transversal direction with the main purpose being to hold the primary fibers in position.

The flexural strength f_{tm} and compressive strength f_{cm} of the mortars were determined at 28 days in accordance with ASTM C348 (2014) and ASTM C349 (2014), respectively. The average results are presented in Table 2.

Strengthening Procedure

The concrete surface was prepared, in accordance with prEN 1504-10 (2015), by water-jetting at 200 MPa (2000 bar) water pressure using a rotating nozzle with five jets. The resulting surface roughness corresponded to concrete surface profile number 5, as defined by ICRI 310.2R (2013).

The consistency of both mortars enabled rendering on vertical surfaces, however, for convenience the composites were applied with specimens resting horizontally, on a wooden platform. During strengthening, 4 mm thick steel plates with widths of 60 and 70 mm, were temporarily attached to the specimen surface along the horizontal (X-axis) and vertical (Y-axis) edges, respectively. This measure was taken to maintain the same supports as for the specimens without strengthening and to allow a better control of the mortar layer thickness.

The first mortar layer was then applied to the concrete, and the bi-directional carbon net was pressed slightly into the fresh mortar. In the case of the PBO net, uni-directional nets were first placed in the horizontal direction, and then in the vertical direction. A second set of steel plates, attached on top of the fiber nets, was used to secure each net in place before applying the external mortar layer. For the first seven days of curing, the specimens were sprayed with water and covered with a plastic foil. This measure was taken to prevent edge-lifting and matrix cracking resulting from shrinkage that occurs when fresh mortar is overlaid on old concrete (D'Antino et al. 2016). Thereafter, the steel plates were removed and the panels were cured under normal ambient conditions (~15°C and 50% relative humidity) for at least 28 days, until the day of testing.

Test Setup

The experimental setup was designed to replicate structural walls subjected to only gravitational loads (i.e., transverse loads or lateral in-plane loads were neglected) and consisted of three main parts, namely, the: (i) reaction frame that was fixed to the strong floor by two pairs of pre-stressed steel rods, (ii) loading unit that consisted of four 1-MN-capacity hydraulic jacks and (iii) support frame that consisted of four components (loading beam, reaction beam, and lateral supports).

The out-of-plane displacement of the specimen was restrained on all four sides, with full rotations allowed along the top and bottom supports. An eccentricity e=10 mm (1/6 of the solid-panel thickness) was provided at the top and bottom sides, to reflect deviations that may be introduced during the construction phase of a building. The eccentrically applied axial load, generates out-of-plane bending deformations in the tested panel, leading to tensile deformations on one face of the panel, hereafter referred to as *tension side*, and compressive stresses on the opposite face, hereafter referred to as *compression side,* see Fig. 1.

The compression load was applied by the hydraulic jacks vertically (Y direction) in displacement-control mode, at a rate of 0.003 mm/s. Two linear variable displacement transducers (LVDTs) placed between the reaction frame (assumed rigid) and the loading beam were used to measure the vertical displacement of the loading beam. The hydraulic pressure provided to the four jacks was adjusted by a control unit, to maintain a loading beam displacement rate of 0.003 mm/s. Additional measurements were performed using two image correlation systems (ICSs), and electric resistance strain gages. The position of the ICSs relative to the tested panels, and an overview of the experimental setup are shown in Fig. 2.

Strain gages were installed on the internal steel reinforcement, and on the fiber bundles on the *tension side*. The gages on the bundles were placed at the same location as those on the reinforcement. Eight, 60-mm-long strain gages were attached to the concrete surface on the *compression side* of the solid wall (Fig. 3). The gages were denoted as $G\#_i^j$ where # represents the locations shown in Fig. 3. The subscript i represents the position [i.e., on the steel reinforcement ($_s$), fiber net ($_f$), or concrete *compression side* surface ($_c$)] of the gages. Similarly, the superscript j represents the global direction (x: horizontal and y: vertical) of the gage. For example, $G1_s^x$ indicates that strain gages were placed at some given location in the horizontal direction on the steel reinforcement. Subscript s,f indicates that the gages are placed on both the steel reinforcement and the fiber bundle.

Digital photogrammetry is a non-contact measurement technique for identifying the coordinates of points and patterns in images obtained using imaging sensors, such as charged-coupled devices (CCD). Based on the targets used, digital photogrammetry techniques are classified as point tracking (PT), digital image correlation (DIC), and target-less approaches (Baqersad et al. 2016). DIC for structural monitoring has been successfully applied by researchers in laboratory and outdoor experimental tests. For example, DIC was used by Mahal et al. (2015) and (Ghorbani et al. 2015) to obtain crack patterns and measure crack openings on RC beams and masonry walls, respectively. DIC was also used by Sas et al. (2012) to obtain the principal strain distribution in the shear span of a bridge tested to failure.

Two stereo ICS, Aramis 5M and Aramis 2M, were used to measure the deformation of the tested specimen and the deformation of the test rig supports (Fig. 2). The setup of the systems was similar and both used lenses with a focal length of 12 mm; however, cameras with 2448 × 2048 pixel resolution and 1600 × 1200 pixel resolution were used for the systems on the *tension side* and on the *compression side*, respectively. A plan view of the ICS positioning relative to the specimen faces is shown in [Fig. 2(a)]. Both systems were calibrated using 40 pictures of a 700 × 560-calibration object in different positions and orientations, for a calibrated measurement volume of 1900 mm (X) × 1685 mm (Y) × 1685 mm (Z). PT was used to determine the out-of-plane displacement at the locations specified in Fig. 3. Optical targets (i.e., 16-mm-diameter stickers consisting of a white disc on a black background) were placed at key locations on the surface of each specimen. The targets were mainly used to provide reference measurements of panel location relative to a coordinate system and to allow the live monitoring of displacements during testing. Points referred to as Ref. 1–Ref. 4 were placed 100 mm from the edge of the panel (see Fig. 3). These points were used as references for defining the origin and orientation of the axes of the global coordinate system (GCS), where X: horizontal axis, Y: vertical axis, and Z: perpendicular to the XY plane. The origin of the GCS is at the west-side bottom corner of the panels in the center of the cross-section. Targets denoted as D1–D7 are placed at locations where the out-of-plane displacement was measured.

For DIC measurements, a white base layer was applied to the surface of the specimen, and a random speckle pattern was subsequently applied using black ink. The image was divided into subsets of 20 × 20 pixels, with a 10-pixel overlap between consecutive facets in both directions [(Fig. 2(b)]. This choice of facet and step size yielded suitable resolution and precision. The calibration deviation of the ICS system was 0.03 pixels. For the measurement volume considered, a displacement precision and a strain precision of 0.05 mm and ~200 μm/m, respectively, were realized.

Experimental Results

A summary of the test results is presented in Table 1. The results are presented as load vs. in-plane and out-of-plane displacements. The strain response of the steel reinforcement, fiber net, and concrete is also presented.

Control Specimen – Solid Wall

Load-displacement Response

The applied load (P)–vertical displacement (δ_y) response and the maximum out-of-plane deformation (δ_z) response are shown in Fig. 4(a). δ_y is computed as the average of the results obtained from the two LVDTs that measure the displacement of the loading beam relative to the reaction frame. δ_z represents the out-of-plane deformation measured at the location where the highest panel-surface deformation values occur consistently (i.e., location D3, see Fig. 3). The maximum load capacity of the panel (P_{max}), and the corresponding δ_y^{Pmax}, and δ_z^{Pmax} values are listed in Table 1.

The P-δ_y response was linear or quasi-linear for loads of up to 95%P_{max}, and non-linear thereafter. Once P_{max} was reached, the failure mechanism was activated, as evidenced by a rapid decrease in P and a sharp increase in δ_z.

Fig. 4(b) shows the out-of-plane deflection profiles obtained from DIC full-field measurements along horizontal (X) and vertical (Y) sections created in the middle of the panel. These profiles are obtained at loads of 1.0 MN, 1.5 MN, 95% P_{max} (1.7 MN), and P_{max} (1.8 MN), panel deformation in both directions occurs in all cases. Along the Y axis, the deformations near the top half of the panel (Y coordinate = 675 mm to 1350 mm) are higher than those at the bottom of the panel (Y coordinate = 0 mm to 675 mm). This indicates that the top support underwent a small translation, whereas the bottom support was fixed. The shape of the deformation profiles is consistent with the pinned-support conditions assumed for both the X and Y directions. The test setup is symmetrical with respect to the X axis. However, the out-of-plane displacement profile along the X section shows a slight dissymmetry, particularly close to P_{max}, with higher values occurring on the east side (X coordinate = 900 mm to 1800 mm). The maximum out-of-plane displacement at P_{max}, measured at the mid-height of the east and west lateral support frames, were 2.90 mm and 2.30 mm, respectively. The difference between the displacement of two support frames can be attributed to different tolerances between bolts and holes in the steel profiles of the two lateral support frames.

Large deflections of the panel, with magnitude denoted by the red area between the displacement profiles [see Fig. 4(b)], were recorded when the load was increased from 95%P_{max} to P_{max}. These deflections are indicative of the impending loss of element stability.

Steel and Concrete Strain Response

Fig. 4(c) shows the strain development in the steel reinforcement bars (four horizontal strain gages $G1_s^x - G4_s^x$ and one vertical strain gage $G5_s^y$) and the DIC-determined principal tensile-strain distribution, at P_{max}, on the *tension side* of the panel surface. In terms of cracking pattern, the tensile-surface strain distribution offers a good representation of the condition of the panel at

P_{max}. At P_{max}, cracks open from the corners of the panels at 20–35° inclination with respect to the vertical axis and progress until continuous cracks arch over the height of the panel on each lateral side at failure.

The strain in the horizontal bars increases slowly with increasing load of up to 95%P_{max}, and rapidly thereafter. $G1_s^x$ and $G4_s^x$, which were closer to the corners of the panel, recorded higher strains at P_{max} than $G2_s^x$ and $G3_s^x$. This concurs with the strain distribution on the *tension side* of the panel, where broader high-strain bands [i.e., red lines in Fig. 4(c)] occur at the corners of the panel than at other locations. The maximum strain in the horizontal-reinforcement measured using strain gages at ultimate load was 2228 μm/m, was close to the yield limit (2830 μm/m). However, owing to the local nature of these measurements, recording of the maximum strain occurring in the reinforcement may be prevented by cracks forming in locations other than the strain-gage position. Therefore, compared with the strain-gage measurements, DIC measurements may better represent the global behavior of the tested panels. Larger cracks were observed on the east side of the wall than on the west side, where all strain gages were installed, suggesting that the reinforcement might have yielded, although, this was not recorded by strain gage measurements.

Compressive strains in the vertical reinforcement (i.e., $G5_s^y$) increased linearly up to 524 μm/m at 95%P_{max}. Thereafter, the strain started to decrease becoming almost zero at P_{max}, and high tensile strains developed rapidly in the vertical bar upon initiation of the failure mechanism. Huang et al. (2015) observed a similar strain response for the vertical reinforcement of OW solid panels, where, at failure, the location of the neutral axis was shown to move toward the *compression side* of the panels.

Fig. 4(d) shows the evolution of the concrete strain on the *compression side* and the principal compression-strain distribution, at P_{max}, obtained using strain gages and DIC, respectively.

Measurements were obtained from all gages except $G11_c^y$, which malfunctioned. Even at P_{max}, the strains measured in the horizontal (X) direction were substantially smaller than those measured in the vertical (Y) direction. In general, the strains measured along the vertical direction increased non-linearly with the applied load. The differences among the readings of $G15_c^y$, $G17_c^y$, and $G13_c^y$ are attributed to the fact that, at failure, only gage $G13_c^y$ intercepted the concrete crushing band. The compressive-strain distribution obtained at P_{max} concurs with the strain gage measurement results. The load is distributed across the entire panel, with a mean strain of 2000 μm/m across the surface, with more pronounced concentrations (of ~2800 μm/m) occurring in the east-top corner than in the other corners. The higher strain concentrations on the east side result from the difference in lateral support displacement. A more uniform strain distribution across the surface of the panel would perhaps lead to a higher maximum capacity of the solid panel.

Failure Mode

After P_{max}, cracks on the *tension side*, progress rapidly from the corners of the panels at 45–50° inclination, with respect to the vertical axis, toward the middle of the panel. Similarly, on the *compression side*, high-compression strain bands progress from the corners of the panel toward the center following the same path as the major cracks on the *tension side* (Fig. 5). The moment immediately preceding failure is denoted by the symbol × on the P-δ_z curve [see Fig. 6(a)]. The failure was similar to that of two-way action concrete plates, characterized by diagonal cracks on the *tension side* and concrete crushing in the corresponding locations on the *compression side*. This observation is consistent with those reported in previous studies (Saheb and Desayi 1990a; Doh and Fragomeni 2005; Popescu et al. 2016). After P_{max}, the load-carrying capacity of the panel decreases, and the vertical displacement increases at a constant rate (0.003 mm/s). Furthermore, the strains on the *compression side* increase continuously toward the center of the panel, cracks on the *tension side* open continuously (Fig. 5). Simultaneously, the out-of-plane displacement increases rapidly [Fig. 4(a)]. At P_{max}, the mean concrete compressive strain on the *compression side* was 2000 µm/m, lower than the concrete strain at peak stress (ε_{c1}=2600 µm/m) calculated according to EC 2 (2005), based on the f_c. This indicates that the panel fails primarily via buckling (Huang et al. 2015). In other words, at failure, the panel becomes unstable and undergoes inelastic buckling.

Strengthened Specimens with Openings

Load-displacement Response

The response of specimens with openings, namely SO1, SO2, LO1, and LO2, is shown in Fig. 6-Fig. 9, respectively. Figs. 6-9(a) show the previously defined P-δ_y and P-δ_z responses. In addition, Figs. 6-9(b) show the out-of-plane deflection profiles obtained from DIC full-field measurements, along X and Y sections created in the middle of the panel. These profiles were obtained at loads of 1.0 MN, 1.5 MN (for panels with *small openings* only), 95%P_{max}, and P_{max} (see Table 1 for the P_{max} associated with each tested panel). The capacity of both SO panels was higher than the capacity of SW (i.e., the target capacity), whereas the capacity of the LO panels was lower.

Up to P_{max}, strengthened panels exhibit a quasi-linear load – vertical deformation (P-δ_y) response. In terms of out-of-plane deformations, for panels with openings, the P-δ_z response is quasi-linear up to about 1.0 MN and non-linear thereafter. The applied load decreases abruptly after P_{max} and, unlike for SW, the strengthened panels all fail when P_{max} is reached.

Like SW, the strengthened panels exhibited double-curvature deformations, which are representative of pinned supports although, due to the openings, the deformed shapes differ from those of SW. Deflection profiles along the horizontal section show a greater dissymmetry, compared with those of SW. Observed out-of-plane deflections of the east side support were 0.9 to 1.4 mm larger than of the west side support, compared to the 0.6 mm difference observed between the two side support of SW. The horizontal deflection profiles of SO panels show a smaller curvature than that corresponding to SW, and the horizontal profiles of the LO panels as well are linear. Moreover, deflections of the LO and SO panels increase gradually (rather than suddenly as in the case of SW) with loads ranging from 95%P_{max} to P_{max}.

Steel and Fiber-bundle Strain Response

Fig. 6-Fig. 9(c) show the strain development in the steel reinforcement bars and the distribution of principal compressive strains, at P_{max}, on the *compression side* of SO1, SO2, LO1, and LO2, respectively. Similarly, Fig. 6–Fig. 9(d) show the strain development in the FRCM fiber bundles and the distribution of principal tensile strains, at P_{max}, on the *tension side* of the panels.

During the concrete surface-preparation process, the water jet cut the wires of strain gages $G1_s^x$ and $G2_s^y$ on panel SO2. Strain gages applied to the fiber bundles all performed measurements, except for $G6_f^x$ and $G2_f^y$ attached to panels LO1 and LO2, respectively. Furthermore, a hard disk drive error occurred during testing, thereby preventing full-field measurements on the *compression side* of the LO2 panels.

In general, the ICS-determined strain distribution revealed, as in the case of the SW panel, higher levels of strain on the east pier of each panel than on the west pier. Tensile strains and compressive strains were measured on the horizontal steel reinforcement and the vertical reinforcement, respectively. Measurements by $G3_s^x$, indicate that in all cases the steel bars yielded or were close to the yield limit (2830 μm/m). However, the strains measured on the horizontal steel reinforcement bars were significantly lower than those measured on SW. Compressive strains were recorded for the vertical steel reinforcement bars, and for panels with openings, these strains were all higher than those measured for SW.

In SO1 and SO2, compressive strains at P_{max} are higher along the edges of the openings than along the lateral supports, consistent with the results obtained for steel reinforcements in SO1 [Fig. 6(c), Fig. 7(c)]. Measurements of the reinforcements revealed that the strains in a vertical bar close to the edge of the opening ($G2_s^y$), are two times higher than those measured close to the middle of the pier ($G5_s^y$).

For specimen LO1, the compressive strain at P_{max} was distributed relatively uniformly over the width of the pier [Fig. 8(c)]. This is consistent with strain measurements on the vertical steel reinforcement, where similar levels of strain occurred at locations $G2_s^y$ and $G5_s^y$ for both LO1 and LO2 panels [Fig. 8(c), Fig. 9(c)].

The strain evolution of the fiber bundles was similar to that of the steel reinforcement, although the strains measured on the bundles were, in general, smaller than those on the reinforcement. The maximum strain recorded for C-FRCM and PBO-FRCM were 716 μm/m and 1171 μm/m, respectively. The strains recorded for PBO-FRCM were in general slightly higher than those associated with C-FRCM. Debonding strains of 5600 μm/m and 10000 μm/m, have been determined from direct lap-shear tests on C-FRCM and PBO-FRCM joints, respectively (Sneed et al. 2014; Sabau et al. 2017). This suggests that the fiber bundles remained bonded to the matrix up to failure.

However, strain-gage measurements are performed on a local level and, for the same applied load, different bundles may experience different levels of strain (Sabau et al. 2017). In addition, strain gages were installed only on the west pier, where strains were generally lower than on the east pier and, hence, the maximum strain in the bundles may have been considerably higher than the measured values. The tensile-strain distribution at P_{max} offers a good representation of the crack patterns immediately preceding failure. The strain distribution on panels with *small openings* indicate that, as in the case of SW, crack-opening began at the corners (at an inclination of 20–30° with respect to the vertical axis) and progressed to the middle of the pier. The strain distribution of panels with *large openings* reveal that crack-opening began at an inclination of 40–50° with respect to the vertical axis. Moreover, the cracks on the top side of the pier and those at the bottom of the pier seem to progress toward the corner of the opening and the mid-height of the pier, respectively. In all cases, strain concentrations occurred at the corners of the openings on the *compression side* and at the corners of the panels on the *tension side*.

Failure Mode

The strengthened panels with openings all failed via concrete crushing at the bottom of the east pier, just above the contact with the reaction beam. In this case, the failure mode differed from that of SW, where failure occurred owing to a loss of panel stability. The failure of the east pier can be attributed to the larger out-of-plane deformations observed here, compared to the west pier. According to Popescu et al. (2016) axially loaded panels with openings collapse when failure of one pier occurs, and the ultimate capacity is obtained by multiplying the capacity of the weakest pier with the total numbers of piers. Therefore, when evaluating the capacity of the panel, the characteristics of the weakest pier (i.e. the pier with the large deformations) are considered.

The FRCM became partially detached in the crushed region and, after the test, removing the FRCM composite from this region, revealed the extent of the crushed zone (see Fig. 10). Concrete aggregates remained attached to the composite indicating that FRCM detachment occurred after concrete crushing. After failure, PBO-FRCM-strengthened panels had finer cracks than their C-

FRCM-strengthened counterparts, as revealed by comparing the strain, at P_{max}, on the *tension side* of the panels.

Discussion

Capacity Enhancement

Both FRCM composites restored the capacity of walls with *small openings* to that of the *solid wall*, see Table 1. However, the capacity of walls with *large openings* was only 75% that of the *solid wall*. Moreover, due to higher dissymmetry observed in the deflection profiles of walls with openings compared to the solid wall, the associated reductions in the panels' capacity are higher for walls with openings. Therefore, the enhancement provided by the FRCM strengthening can be seen as a lower bound, with higher capacity increments achievable for cases when deformations are more evenly distributed between to piers.

Axial strength enhancement is defined as the ratio of the capacity associated with a strengthened element to the capacity of a reference element, usually the same type of element before strengthening. The reference values are determined based on the results of a recent experimental study conducted by the authors (Popescu et al. 2016), where the effect of cutout openings on the axial strength of similar panels was investigated. Reference values (SO^{ref} and LO^{ref}) corresponding to 36% and 50% of the capacity of SW (see Table 1 and Fig. 11) were obtained for the panels with *small openings* and *large openings*, respectively.

The capacity of SO specimens strengthened with C-FRCM and PBO-FRCM were 185% and 161% of reference capacities, respectively. The capacity of LO specimens strengthened with C-FRCM and PBO-FRCM was 148% and 150% of the reference capacities, respectively. Because the failure mode (concrete crushing) remained unchanged for all strengthened panels, the differences in strength enhancement between C-FRCM and PBO-FRCM for the same type of panel are attributed to the normal variations of concrete material properties and possible variations in the boundary conditions.

Stiffness Enhancement

Fig. 11(a) shows the applied load vs. the out-of-plane displacement measured at location D1 (δ_z^{D1}),on all the tested specimens. As the figure shows, the stiffness of the strengthened LO panels is restored to that of the SW panel, and the stiffness of the SO panels is higher than that of the SW panel. These results concur with those of studies, where masonry panels that were strengthened with FRCM on only the *tension side* and tested in one-way action exhibited higher stiffness than the non-strengthened panels (Escrig et al. 2015). Therefore, the stiffness increase can be attributed primarily to the FRCM layer applied on the *tension side*, although, the reduction of the eccentricity relative to the panel thickness might also play a significant role in this case. The rigidity of the element against out-of-plane deformations is important in reducing the influence of second-order effects and increasing the capacity of the elements.

In terms of existing structures, changes in the axial rigidity of wall panels influences the distribution of load between vertical load-bearing elements. The axial rigidity of a panel may be reduced by cutout openings. However, to the authors' knowledge, the influence of openings on the axial rigidity has yet to be reported. Fig. 11b compares the load – δ_y response of the tested specimens. As the figure shows, the axial stiffness of SO panels matched that of the SW panel, whereas the stiffness of LO panels was lower. Further studies are needed to determine the influence of openings and strengthening solutions the axial stiffness of concrete panels.

Ultimate capacity analysis

In this section a comparison is made between experimentally obtained capacity and predictions of analytical models proposed by Doh and Fragomeni (2005) for the solid walls and by Guan et al. (2010) for walls with openings. The chosen models were previously shown by Popescu et al. (2015) to outperform current design codes in terms of accuracy. It should be noted that the models, were not developed for walls with strengthening, therefore a perfect agreement between experimental and theoretical values of ultimate capacities was not expected. However, the strengthened panels could be considered as having two layers of reinforcement, placed symmetrically on each face, and treated as a normal RC wall with an opening.

Doh and Fragomeni (2005) proposed a semi empirical equation for predicting the ultimate load (N_u) capacity of low and high strength concrete walls supported on two or four sides, with a slenderness ratio H/t ≤40, and aspect ratio 0.5≤H/L≤1.6:

$$N_u = 2f_c^{0.7}(t - 1.2e - 2e_a)L \tag{1}$$

where f_c is the concrete compressive strength, t is the panel thickness, e is the initial load eccentricity, e_a is an additional eccentricity that accounts for the effect of slenderness, also known as second-order effects, and L is the length of the wall, as shown in Fig. 12.

The additional eccentricity e_a, can be estimated as:

$$e_a = \frac{(\beta H)^2}{2500t} \tag{2}$$

where β is the effective height factor that takes into account the aspect ratio and the boundary conditions. For walls restrained on four sides and having H<L:

$$\beta = \begin{cases} \alpha \dfrac{1}{1 + \left(\dfrac{H}{L}\right)^2} \; for\ H \leq L \\ \alpha \dfrac{L}{2H} \qquad for\ H > L \end{cases} \tag{3}$$

where α is an eccentricity parameter:

$$\alpha = \begin{cases} \dfrac{1}{1-\frac{e}{t}} & for \ \dfrac{H}{t} < 27 \\ \dfrac{1}{1-\frac{e}{t}} \cdot \dfrac{18}{\left(\frac{H}{t}\right)^{0.88}} & for \ \dfrac{H}{t} > 27 \end{cases} \tag{4}$$

Doh and Fragomeni (2005) modified the effective height factor by incorporating parameter α to the factors available in EC 2 (2005) and AS 3600 (2009).

Guan et al. (2010) updated the formula initially proposed by Saheb and Desayi (1990b), for walls with openings, by incorporating an opening parameter that considers the combined effects of the openings' height, length, and location:

$$N_{uo} = \left(k_1 - k_2\alpha_{xy}\right)N_u \tag{5}$$

where, N_u is the capacity of an identical solid panel, and α_{xy} is the opening parameter:

$$\alpha_{xy} = \frac{\alpha_x + \lambda\alpha_y}{1+\lambda} \tag{6}$$

with,

$$\alpha_x = \frac{L_o + d_x}{L} \tag{7}$$

and

$$\alpha_y = \frac{H_o + d_y}{H} \tag{8}$$

assuming a constant wall thickness, *t*. All terms in Eq. (6-8) can be determined from Fig. 12. In Eq. (5), $k_1 = 1.358$ and $k_2 = 1.795$ are constants determined through linear regression analysis.

Eq. (2) provides the theoretical value of the additional eccentricity (e_a^{th}). Furthermore, the additional eccentricity was determined experimentally (e_a^{exp}), as the maximum out of plane displacement of each panel, at failure, δ_z^{Pmax}. Values of e_a^{th} and e_a^{exp} are given in Table 3.

The maximum capacity of the tested panels, P_{max}, and the predictions given by Eq. (1) for the solid wall and Eq. (5) for walls with openings (i.e. N^{th} and N^{mod}, considering e_a^{th} and e_a^{exp}, respectively) are given in Table 3. (i.e. N_u^{th} and N_u^{mod}, considering e_a^{th} and e_a^{exp}, respectively). In all cases, t is taken as the measured total panel thickness (i.e. for the strengthened panels t includes the thickness of the FRCM strengthening).

Solid wall

As can be seen from Table 3, N_u^{th} overestimates P_{max} by 29%. This can be explained by the fact that e_a^{th} underestimates the second order effects. According to EC 2 (2005), β should be factored by 0.85 when the panels' restrains are flexural rigid. This suggests that the Equation 3 should be valid for panels having rotational capacity at the restraints. The deflection profiles in Fig. 4b indicate a curvature of the panel characteristic of elements with pinned supports. Moreover, considering e_a^{exp}, N_u^{mod} gives a safe estimate of the capacity, 16% less than P_{max}. This indicates that e_a has an important influence on the ultimate capacity of wall panels and indicates that the current design equations greatly underestimate the value of e_a, leading to unsafe predictions.

Walls with openings

It can be observed in Table 3 that N_{uo}^{th} overestimates the capacity of SO1 and SO2 panels by 11% and 27%, respectively. Similar to the solid wall, the e_a^{th} underestimates the maximum deformation of the elements. Moreover, N_{uo}^{mod} provided a better estimate of the capacity, 5% less than P_{max} for SO1 and 10% higher than P_{max} for SO2.

For LO panels, P_{max} was approximately 25% higher than N_{uo}^{th}. While also in this case e_a^{th} underestimates the deflection of the panels, when considering e_a^{exp}, N_{uo}^{mod} does not show a significantly better performance compared to N_{uo}^{th}. This is in agreement with previous studies (Popescu et al. 2016) where it was shown that the effect of the initial eccentricity, e, weaker for elements with large openings. Similarly it appears that also the effect of the additional eccentricity, e_a, seems to be less important for elements with large openings.

Using e_a^{exp}, the studied models provided capacities mostly on the safe side. Therefore, using suitable safety factors, the model can be used in estimating the capacity of FRCM strengthened TW panels with openings. However, design models for axially loaded TW panels are mostly empirical and developed based on a limited of experimental tests, therefore are not always directly applicable in practice.

Numerical models can be used to study the influence several parameters such as slenderness, boundary conditions and reinforcement layout, on the capacity of RC panels with openings (Ho et al. 2016). In addition, numerical models can be used to quantify the influence of parameters pertaining to the FRCM strengthening such as, layer thickness, fiber reinforcement ratio, and mortar strength (Wang et al. 2017). Thus, numerical models can be used to provide a basis for the further refinement of existing empirical equations trough factors considering the abovementioned parameters. However, to provide reliable results numerical models should be verified using experimental tests such as reported herein.

Alternatively, models based on observed failure modes, that can consider the actual deformation of TW action panels and the properties of constituent materials (i.e. concrete, steel reinforcement, FRCM composites) should be developed. For example, a general analytical approach based on concrete plasticity and limit state design was recently proposed by Popescu et al. (2017b) for walls with openings strengthened by FRP confinement.

Contribution of FRCM strengthening

The contribution of the FRCM can be considered from two perspectives, geometrical and mechanical. The geometrical contribution is considered the capacity increase resulting from changes in the geometrical properties of the panel. For example, with FRCM strengthening on both sides of the panel, the panel thickness increased, on average, by 27% (from 60 mm to 82 mm), whereas the element slenderness decreased (from 22.5 to 16.5). In turn, the eccentricity ratio decreased from *t/6* to *~t/8*, relative to the new panel thickness.

The mechanical contribution is considered the FRCM-composite-induced increase in the axial and moment capacity of the cross-section. The additional fiber reinforcement results in increased resistance to crack opening on the *tension side*, and the additional mortar layer on the *compression side* yields increased cross-sectional area under compression.

Table 3 shows that that the predicted ultimate loads N_{u}^{mod} and N_{uo}^{mod} were in reasonable correlation with experimental maximum loads for SW and SO panels, respectively. However for LO panels, N_{x}^{mod} significantly underestimate the maximum capacity of the panel. This can be explained by the fact that the current models only take into consideration the geometrical contribution of the strengthening and cannot account for the mechanical contribution of the FRCM composite. Thus, for LO panels the mechanical contribution of the FRCM strengthening can be estimated as the difference between, P_{max}, and N_{uo}^{mod}, which represent approximately 28% of the experimentally obtained capacity.

For SO panels, it appears that the FRCM composite on the tension side does not provide any mechanical contribution. However, in this case, the contribution of the FRCM composite in tension might be less compared to the geometrical contribution or the design model overestimates the geometrical contribution of the increased panel section. Further studies are necessary to confirm these observations.

Conclusions

RC walls with openings acting as compression members strengthened with FRCM composites were experimentally investigated. To the authors' knowledge, similar tests on FRCM-strengthened concrete walls have yet to be reported. The present work constitutes a first step in establishing FRCM systems as reliable solutions for strengthening concrete panels with cutout openings acting as compression members. Four FRCM-strengthened panels with openings and one solid non-strengthened panel were tested to failure under eccentric compression. Image correlation systems were used to monitor the full surface of both sides of the tested panels. The test results were discussed from the viewpoint of the observed failure modes and displacement response, as well as strain measurements on the steel reinforcement, fiber bundles, and the surface of the tested panels. The appropriateness of existing design methods RC panels has been assessed in comparison with the experimental results.

The following conclusions are drawn based on the findings of this study. Owing to the FRCM strengthening solution:

- the capacity of the solid wall for panels with small openings was fully restored. However, for panels with large openings the capacity was restored to 75% of the value associated with the solid wall,
- the capacity of panels with small and large openings were 161–185% and 148–150%, respectively, the capacities of their non-strengthened reference counterparts,
- the failure mode of the panels changed from inelastic plate-buckling failure to concrete crushing at the bottom of one pier.

Furthermore,

- concrete crushing occurred on the *compression side* before the maximum tensile strength of the FRCM composites on the *tension side* was reached. This suggests that a lower amount of fiber reinforcement, compared with the amount used, would have provided the same capacity enhancement.
- the strengthening solution yielded both increased in-plane and out-of-plane rigidity of the panels. The out-of-plane rigidity of the solid wall was restored for all panels, whereas the in-plane plane rigidity was only matched for panels with *small openings*.
- the available design methods underestimate the influence of second order effects in the design of solid panels and panels with openings, by providing theoretical values for additional eccentricity significantly smaller than the ones observed in this study. The design models provided a better agreement with the test results when experimental additional eccentricity was used instead of the theoretical one.

The findings of this study indicate that a FRCM strengthening solution can be used for the repair and strengthening of RC panels with cutout openings, and provide foundations for future research.

The conclusions of this work are based on limited experimental tests performed under short-term loading and, hence, generalization based on these conclusions must be avoided. Finite element numerical models can facilitate essential further research on the influence of an increased range of parameters, such as size of openings, FRCM reinforcement ratio, and support conditions.

Acknowledgements

This work was supported by the European Commission (Contract number MC-ITN-2013-607851) and Development Fund of the Swedish Construction Industry (SBUF). The first author would like to acknowledge the support of the European Network for Durable Reinforcement and

Rehabilitation Solutions (endure). The assistance of the technicians at CompLab, the structural engineering laboratory at Luleå University of Technology (LTU), and of Jaime Gonzalez and Carlo Pellegrino from the University of Padova is also gratefully acknowledged.

References

Assefa, G., and Ambler, C. (2017). "To demolish or not to demolish: Life cycle consideration of repurposing buildings." *SCS*, 10.1016/j.scs.2016.09.011, 28, 146-153.

ASTM International. (2014) "Standard Test Method for Flexural Strength of Hydraulic-Cement Mortars." ASTM:C348-14, West Conshohocken, PA, United States.

ASTM International. (2014) "Standard Test Method for Compressive Strength of Hydraulic-Cement Mortars (Using Portions of Prisms Broken in Flexure)." ASTM:C349-14, West Conshohocken, PA, United States.

ASTM International. (2007) "Standard Test Methods for Linear Density of Textile Fibers." ASTM:D1577-07, West Conshohocken, PA, United States.

Babaeidarabad, S., Caso, F. D., and Nanni, A. (2014). "Out-of-plane behavior of URM walls strengthened with fabric-reinforced cementitious matrix composite." *Journal of Composites for Construction*, 10.1061/(ASCE)CC.1943-5614.0000457, 18(4), 04013057.

Baqersad, J., Poozesh, P., Niezrecki, C., and Avitabile, P. (2016). "Photogrammetry and optical methods in structural dynamics – A review." *MSSP*, 10.1016/j.ymssp.2016.02.011.

Bernat, E., Gil, L., Roca, P., and Escrig, C. (2013). "Experimental and analytical study of TRM strengthened brickwork walls under eccentric compressive loading." *Construction and Building Materials*, 10.1016/j.conbuildmat.2013.03.006, 44, 35-47.

Cevallos, O. A., Olivito, R. S., Codispoti, R., and Ombres, L. (2015). "Flax and polyparaphenylene benzobisoxazole cementitious composites for the strengthening of masonry elements subjected to eccentric loading." *Composites Part B-Engineering*, 10.1016/j.compositesb.2014.10.055, 71, 82-95.

Colajanni, P., De Domenico, F., Recupero, A., and Spinella, N. (2014). "Concrete columns confined with fibre reinforced cementitious mortars: Experimentation and modelling." *Construction and Building Materials*, 10.1016/j.conbuildmat.2013.11.048, 52, 375-384.

D'Ambrisi, A., and Focacci, F. (2011). "Flexural Strengthening of RC Beams with Cement-Based Composites." *Journal of Composites for Construction*, 10.1061/(asce)cc.1943-5614.0000218, 15(5), 707-720.

D'Antino, T., Sneed, L. H., Carloni, C., and Pellegrino, C. (2016). "Effect of the inherent eccentricity in single-lap direct-shear tests of PBO FRCM-concrete joints." *Composite Structures*, 10.1016/j.compstruct.2016.01.076, 142, 117-129.

Doh, J. H., and Fragomeni, S. (2005). "Evaluation of Experimental Work on Concrete Walls in One and Two-Way Action." *Aust. J. Struct. Eng.*, 10.1080/13287982.2005.11464943, 6(1), 37-52.

European Committee for Standardization (CEN). (2005) "Eurocode 2: Design of concrete structures." EC 2, Brussels, B-1050, Belgium.

Elsanadedy, H. M., Almusallam, T. H., Alsayed, S. H., and Al-Salloum, Y. A. (2013). "Flexural strengthening of RC beams using textile reinforced mortar – Experimental and numerical study." *Composite Structures*, 10.1016/j.compstruct.2012.09.053, 97(0), 40-55.

European Committee for Standardization (CEN). (2009) "Testing hardened concrete – Part 3: Compressive strength of test specimens." EN ISO 12390-3:2009, Brussels, B-1000, Belgium.

European Committee for Standardization (CEN). (2010) "Steel for the reinforcement and prestressing of concrete - Test methods." EN ISO 15630-2:2010, Brussels, B-1000, Belgium.

Escrig, C., Gil, L., Bernat-Maso, E., and Puigvert, F. (2015). "Experimental and analytical study of reinforced concrete beams shear strengthened with different types of textile-reinforced mortar." *Construction and Building Materials*, 10.1016/j.conbuildmat.2015.03.013, 83, 248-260.

Ferreira, J., DuartePinheiro, M., and de Brito, J. (2015). "Economic and environmental savings of structural buildings refurbishment with demolition and reconstruction - A Portuguese benchmarking." *J. Build. Eng.*, 10.1016/j.jobe.2015.07.001, 3, 114-126.

Ghorbani, R., Matta, F., and Sutton, M. A. (2015). "Full-Field Deformation Measurement and Crack Mapping on Confined Masonry Walls Using Digital Image Correlation." *Experimental Mechanics*, 10.1007/s11340-014-9906-y, 55(1), 227-243.

Gonzalez-Libreros, J. H., Sabau, C., Sneed, L. H., Pellegrino, C., and Sas, G. (2017a). "State of research on shear strengthening of RC beams with FRCM composites." *Construction and Building Materials*, 10.1016/j.conbuildmat.2017.05.128, 149, 444-458.

Gonzalez-Libreros, J. H., Sneed, L. H., D'Antino, T., and Pellegrino, C. (2017b). "Behavior of RC beams strengthened in shear with FRP and FRCM composites." *Engineering Structures*, 10.1016/j.engstruct.2017.07.084, 150, 830-842.

Guan, H., Cooper, C., and Lee, D.-J. (2010). "Ultimate strength analysis of normal and high strength concrete wall panels with varying opening configurations." *Engineering Structures*, 10.1016/j.engstruct.2010.01.012, 32(5), 1341-1355.

Ho, N. M., Lima, M. M., and Doh, J. H. (2016). "Axially loaded three-side restrained reinforced concrete walls: A comparative study." *Mechanics of Structures and Materials: Advancements and Challenges*, CRC Press, 63-72.

Huang, Y., Hamed, E., Chang, Z., and Foster, S. J. (2015). "Theoretical and Experimental Investigation of Failure Behavior of One-Way High-Strength Concrete Wall Panels." *Journal of Structural Engineering*, 10.1061/(ASCE)ST.1943-541X.0001072, 141(5), 04014143.

International Concrete Repair Institute. (2013) "Selecting and Specifying Concrete Surface Preparation for Sealers, Coatings, Polymer Overlays, and Concrete Repair." ICRI 310.2R-2013, Rosemont, IL 60018, USA.

Ismail, N., and Ingham, J. M. (2016). "In-plane and out-of-plane testing of unreinforced masonry walls strengthened using polymer textile reinforced mortar." *Engineering Structures*, 10.1016/j.engstruct.2016.03.041, 118, 167-177.

Kolsch, H. (1998). "Carbon fiber cement matrix (CFCM) overlay system for masonry strengthening." *Journal of Composites for Construction*, 10.1061/(ASCE)1090-0268(1998)2:2(105), 2(2), 105-109.

Mahal, M., Blanksvärd, T., Täljsten, B., and Sas, G. (2015). "Using digital image correlation to evaluate fatigue behavior of strengthened reinforced concrete beams." *Engineering Structures*, 10.1016/j.engstruct.2015.10.017, 105, 277-288.

Mohammed, B. S., Ean, L. W., and Malek, M. A. (2013). "One way RC wall panels with openings strengthened with CFRP." *Construction and Building Materials*, 10.1016/j.conbuildmat.2012.11.080, 40, 575-583.

Ombres, L., and Verre, S. (2015). "Structural behaviour of fabric reinforced cementitious matrix (FRCM) strengthened concrete columns under eccentric loading." *Composites Part B-Engineering*, 10.1016/j.compositesb.2015.01.042, 75, 235-249.

Papanicolaou, C. G., Triantafillou, T. C., Karlos, K., and Papathanasiou, M. (2007). "Textile-reinforced mortar (TRM) versus FRP as strengthening material of URM walls: In-plane cyclic loading." *Mater Struct*, 10.1617/s11527-006-9207-8, 40(10), 1081-1097.

Popescu, C., Sas, G., Blanksvärd, T., and Täljsten, B. (2015). "Concrete walls weakened by openings as compression members: A review." *Engineering Structures*, 10.1016/j.engstruct.2015.02.006, 89, 172-190.

Popescu, C., Sas, G., Blanksvärd, T., and Täljsten, B. (2017a). "Concrete Walls with Cutout Openings Strengthened by FRP Confinement." *Journal of Composites for Construction*, doi:10.1061/(ASCE)CC.1943-5614.0000759, 21(3), 04016106.

Popescu, C., Sas, G., Sabau, C., and Blanksvärd, T. (2016). "Effect of Cut-Out Openings on the Axial Strength of Concrete Walls." *Journal of Structural Engineering*, 10.1061/(ASCE)ST.1943-541X.0001558, 142(11), 04016100.

Popescu, C., Schmidt, J. W., Goltermann, P., and Sas, G. (2017b). "Assessment of RC walls with cut-out openings strengthened by FRP composites using a rigid-plastic approach." *Engineering Structures*, 10.1016/j.engstruct.2017.07.069, 150, 585-598.

European Committee for Standardization. (2015) "Products and systems for the protection and repair of concrete structures - Definitions, requirements, quality control and evaluation of conformity." prEN 1504-10:2015, Brussels, B-1000, Belgium.

Sabau, C., Gonzalez-Libreros, J. H., Sneed, L. H., Sas, G., Pellegrino, C., and Täljsten, B. (2017). "Use of image correlation system to study the bond behavior of FRCM-concrete joints." *Mater Struct*, 10.1617/s11527-017-1036-4, 50(3), 172.

Saheb, S. M., and Desayi, P. (1990a). "Ultimate Strength of R.C. Wall Panels in Two- Way In-Plane Action." *Journal of Structural Engineering*, 10.1061/(ASCE)0733-9445(1990)116:5(1384), 116(5), 1384-1402.

Saheb, S. M., and Desayi, P. (1990b). "Ultimate Strength of RC Wall Panels with Openings." *Journal of Structural Engineering*, doi:10.1061/(ASCE)0733-9445(1990)116:6(1565), 116(6), 1565-1577.

Sas, G., Blanksvard, T., Enochsson, O., Taljsten, B., and Elfgren, L. (2012). "Photographic strain monitoring during full-scale failure testing of Ornskoldsvik bridge." *Struct Health Monit*, 10.1177/1475921712438568, 11(4), 489-498.

Sneed, L. H., D'Antino, T., and Carloni, C. (2014). "Investigation of Bond Behavior of Polyparaphenylene Benzobisoxazole Fiber-Reinforced Cementitious Matrix Composite-Concrete Interface." *ACI Materials Journal*, 10.14359.51686604, 111(5), 569-580.

Sneed, L. H., Verre, S., Carloni, C., and Ombres, L. (2016). "Flexural behavior of RC beams strengthened with steel-FRCM composite." *Engineering Structures*, 10.1016/j.engstruct.2016.09.006, 127, 686-699.

Standards Australia. (2009) "Australian Standard for Concrete Structures." AS 3600, Sydney, Australia.

Todut, C., Dan, D., and Stoian, V. (2015). "Numerical and experimental investigation on seismically damaged reinforced concrete wall panels retrofitted with FRP composites." *Comp. Struct.*, 10.1016/j.compstruct.2014.09.047, 119, 648-665.

Täljsten, B., and Blanksvärd, T. (2007). "Mineral-Based Bonding of Carbon FRP to Strengthen Concrete Structures." *Journal of Composites for Construction*, 10.1061/(ASCE)1090-0268(2007)11:2(120), 11(2), 120-128.

Wang, X., Ghiassi, B., Oliveira, D. V., and Lam, C. C. (2017). "Modelling the nonlinear behaviour of masonry walls strengthened with textile reinforced mortars." *Engineering Structures*, 10.1016/j.engstruct.2016.12.029, 134, 11-24.

Table 1. Summary of Tested Specimens

Specimen	Strengthening system	P_{max} (MN)	$\frac{P_{max}}{P_{max}^{SW}}$	P_{max}^{ref} (MN)	$\frac{P_{max}}{P_{max}^{ref}}$	δ_y^{Pmax} (mm)	δ_z^{Pmax} (mm)	Failure mode*
SW	-	1.80	100%	-	-	8.1	12.8	IB
SO1	C-FRCM	2.13	118%	1.15	185%	8.6	9.0	CC
LO1	C-FRCM	1.33	74%	0.90	148%	7.9	5.8	CC
SO2	PBO-FRCM	1.86	103%	1.15	161%	7.6	8.8	CC
LO2	PBO-FRCM	1.35	75%	0.90	150%	8.2	6.7	CC

Note: IB – inelastic buckling; CC – concrete crushing; P_{max} – maximum applied load; P_{max}^{SW} – maximum capacity of control wall (solid wall); P_{max}^{ref} – reference capacity for panels with openings without strengthening, based on results of Popescu et al. (2016); δ_y^{Pmax} – vertical deformation at P_{max}; δ_z^{Pmax} – maximum out-of-plane deformation at P_{max}

Table 2

Table 2. FRCM Composite Properties

FRCM system	b_f (mm)	A_b* (mm^2)	t_f^1 (mm)	γ (g/cm^3)	b* (mm)	t* (mm)	f_f^1 (MPa)	ε_f^1 (%)	E_f^1 (GPa)	f_{cm} (MPa)	f_{tm} (MPa)	E_{cm}^1 (GPa)
C-FRCM	20 × 20	1.057	0.0460	1.60	3	0.313	4700	18	240	37.8	4.96	15
PBO-FRCM	3 × 12	0.46	0.0455	1.56	5	0.092	5800	21.5	270	46.6	5.00	7

Note: [1]Value reported by the manufacturer

Table 3

Table 3. Comparison Between Experimental and Predicted Maximum Loads

Specimen	P_{max} (MN)	t (mm)	e_a^{th} (mm)	e_a^{exp} (mm)	N_u^{th} (MN)	N_{uo}^{th} (MN)	N^{th}/P_{max}	N^{mod} (MN)	N^{mod}/P_{max}
SW	1.80	60	7.17	12.8	2.32		1.29	1.54	0.86
SO1	2.13	82	4.72	9.0		2.36	1.11	2.02	0.95
SO2	1.86	82	4.72	8.8		2.36	1.27	2.04	1.10
LO1	1.33	82	4.72	5.8		1.02	0.77	0.98	0.74
LO2	1.35	82	4.72	6.7		1.02	0.76	0.95	0.71

Note: N^{th} is N_u^{th} for the solid panel and N_{uo}^{th} for panels with openings calculated using e_a^{th}
N^{mod} is N_u^{mod} for the solid panel and N_{uo}^{mod} for panels with openings calculated using e_a^{exp}

Fig. 1. Geometry, reinforcement and strengthening detail of tested wall panels (dimensions in mm)

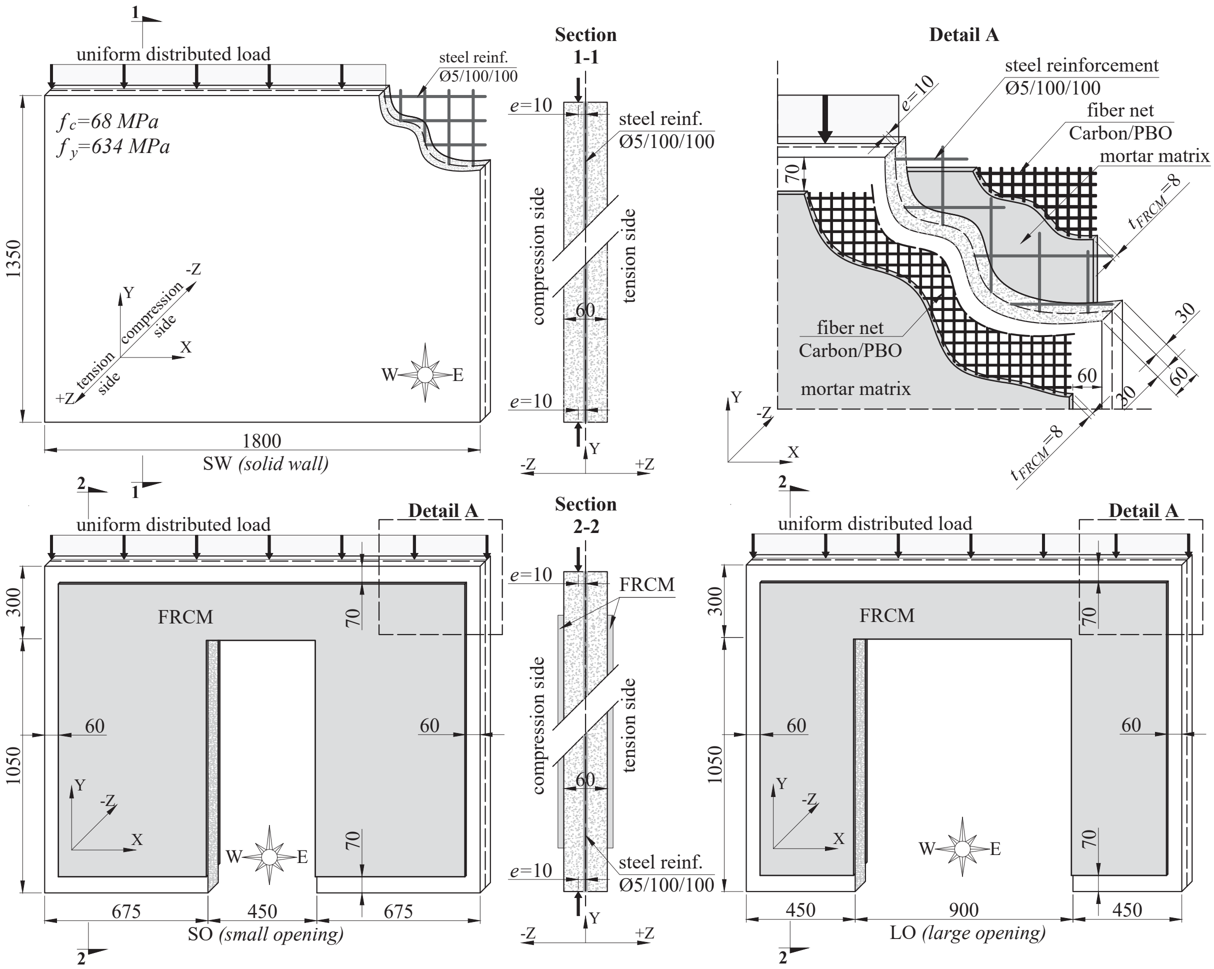

Fig. 2. (a) Schematic of ICS setup (dimensions in millimeters);
(b) overview of setup - Panel LO1 (color)

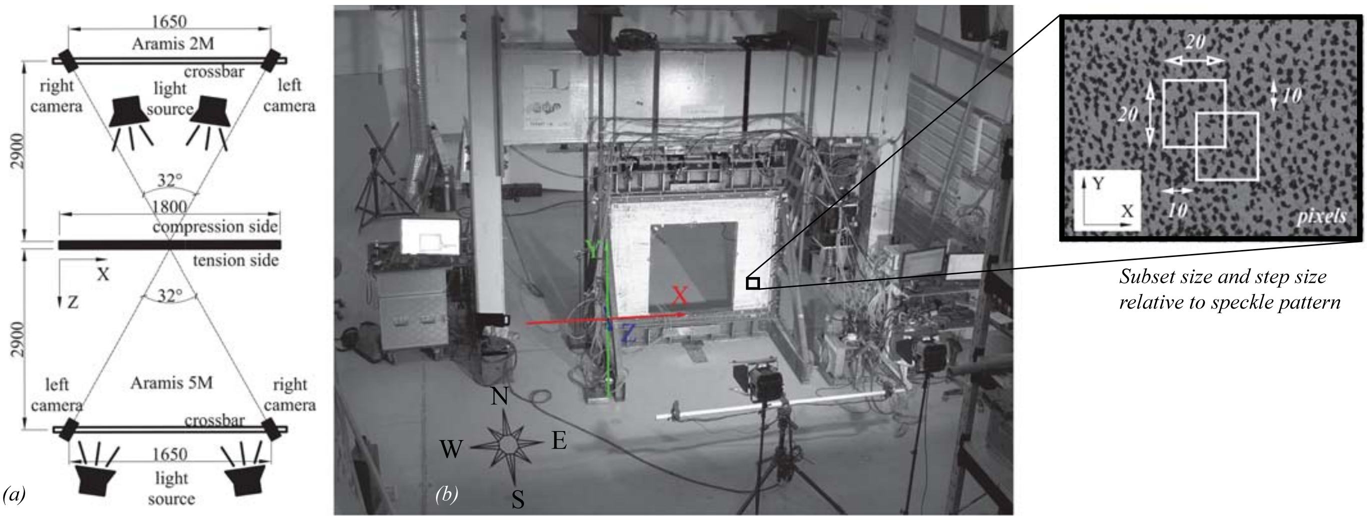

Fig. 3. Instrumentation of each specimen type relative to the global coordinate system (color)

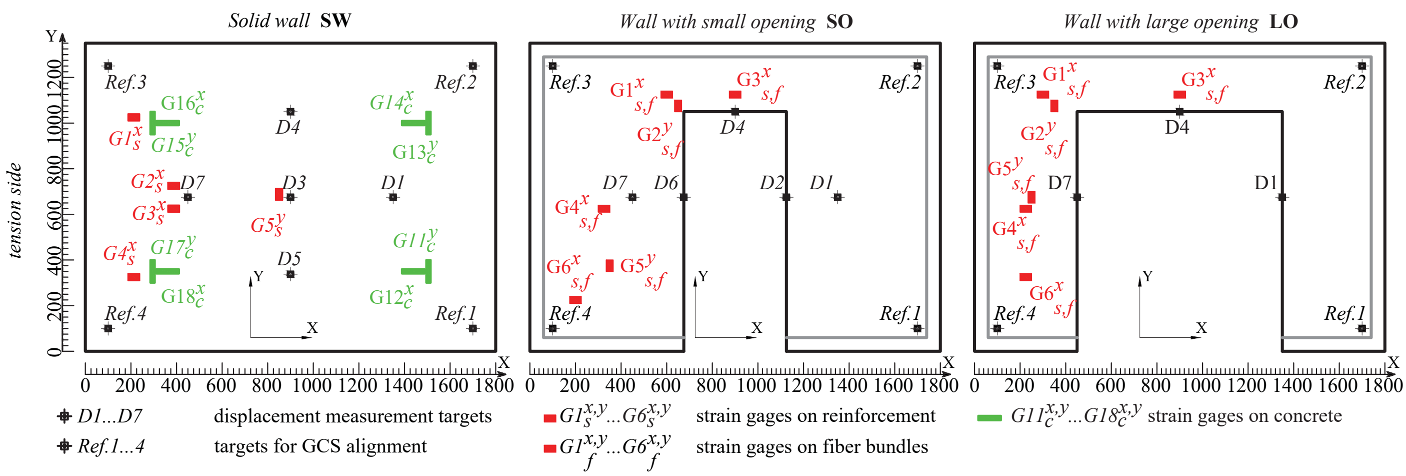

Fig. 4. Response of SW: (a) load vs. δy and δz; (b) out-of-plane displacement profiles; (c) load vs. steel strain and tensile strain

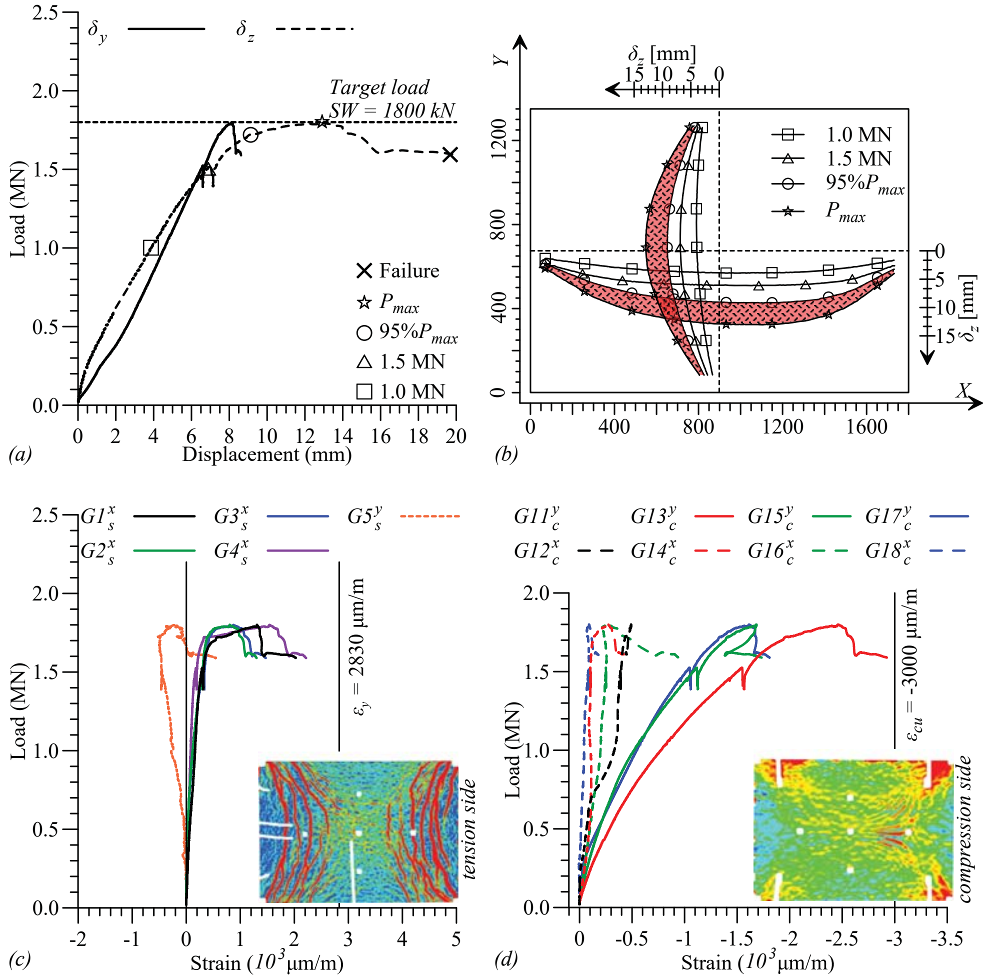

Fig. 5. Surface strain distribution at maximum and failure loads (color)

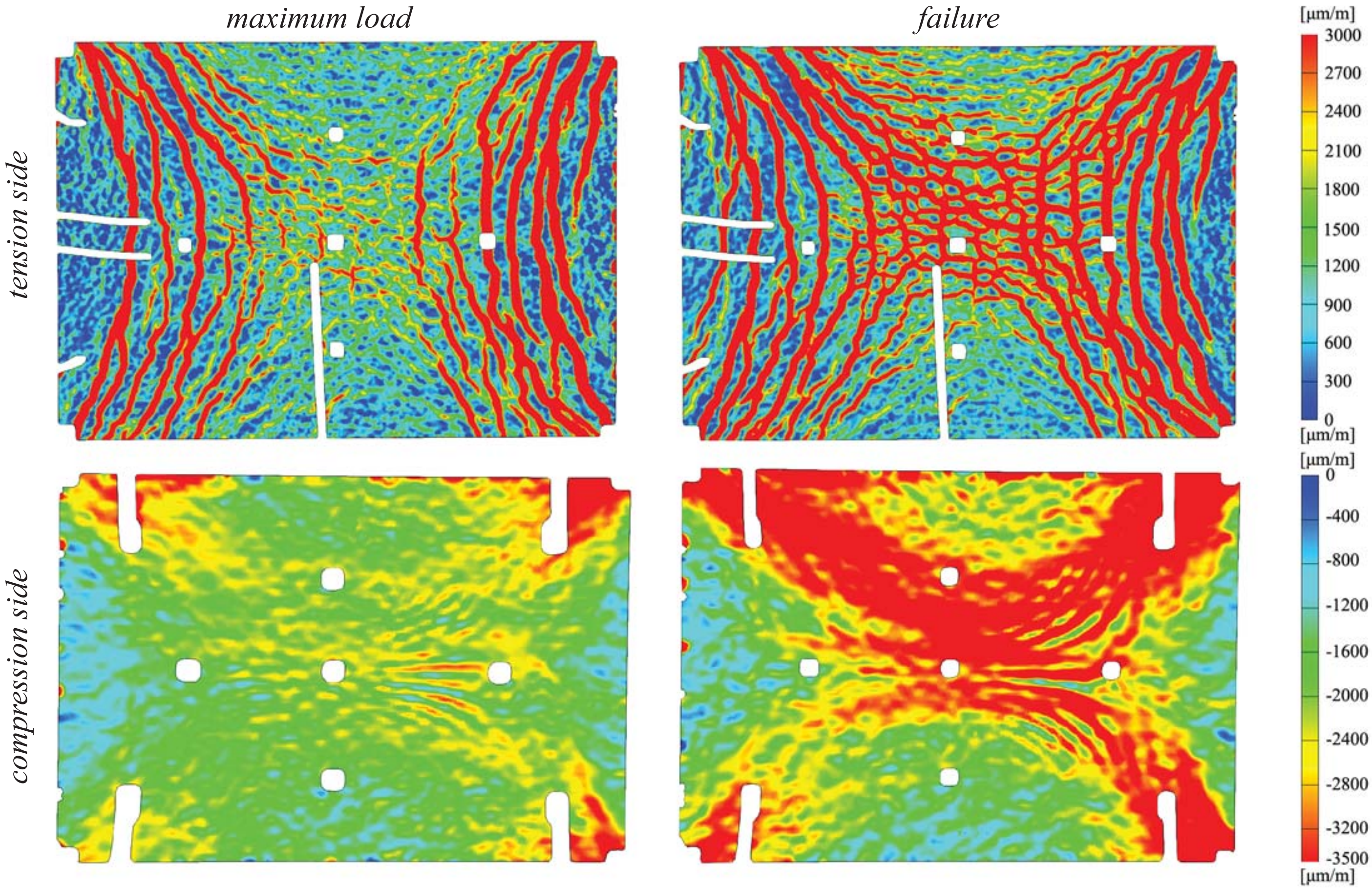

Fig. 6. Response of SO1: (a) load vs. δy and δz; (b) out-of-plane displacement profile; (c) load vs. steel strain and tensile strain

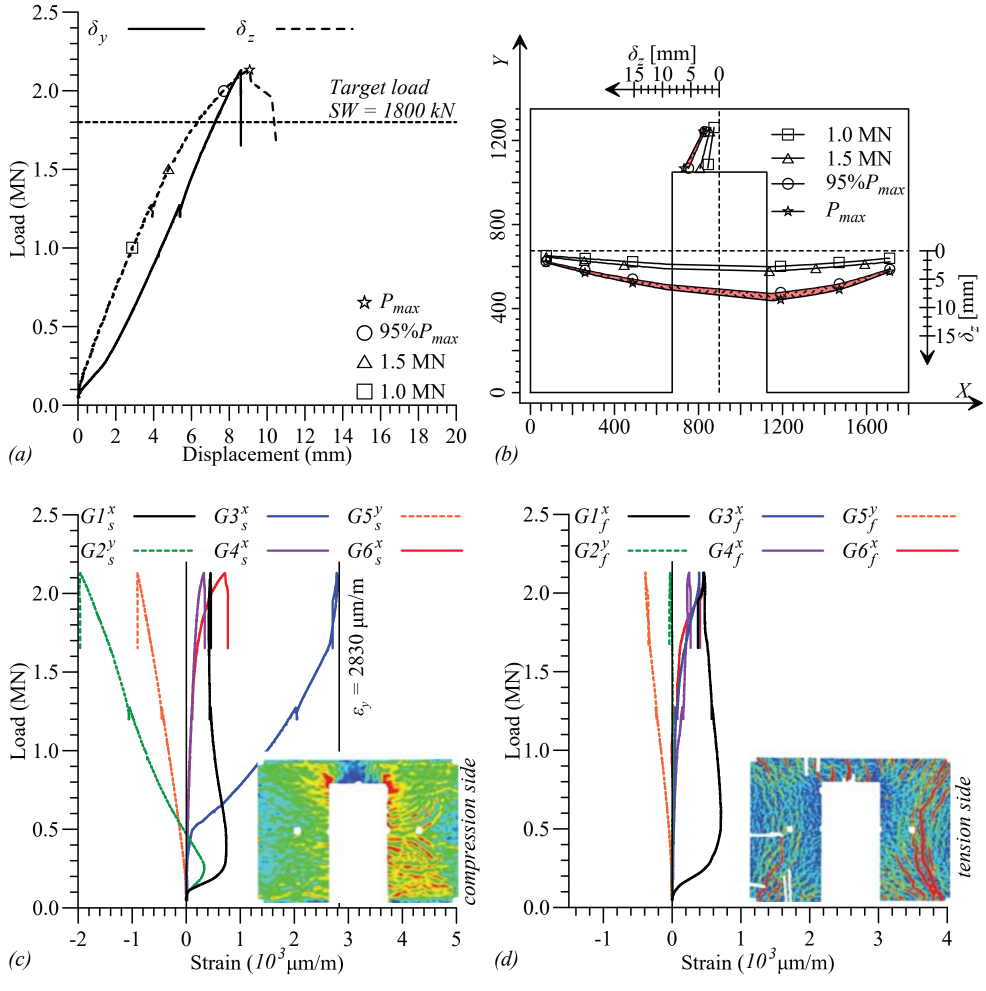

Fig. 7. Response of SO2: (a) load vs. δy and δz; (b) out-of-plane displacement profile; (c) load vs. steel strain and tensile strain

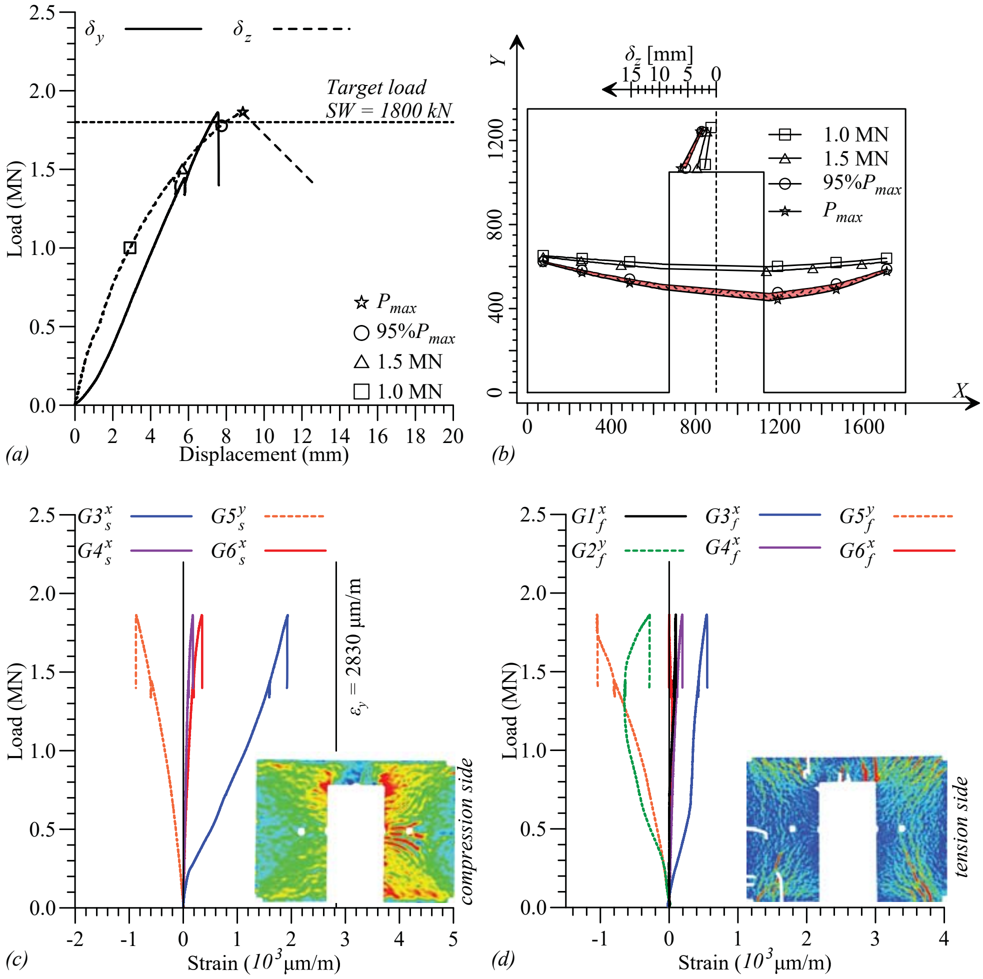

Fig. 8. Response of LO1: (a) load vs. δy and δz; (b) out-of-plane displacement profile; (c) load vs. steel strain and tensile strain

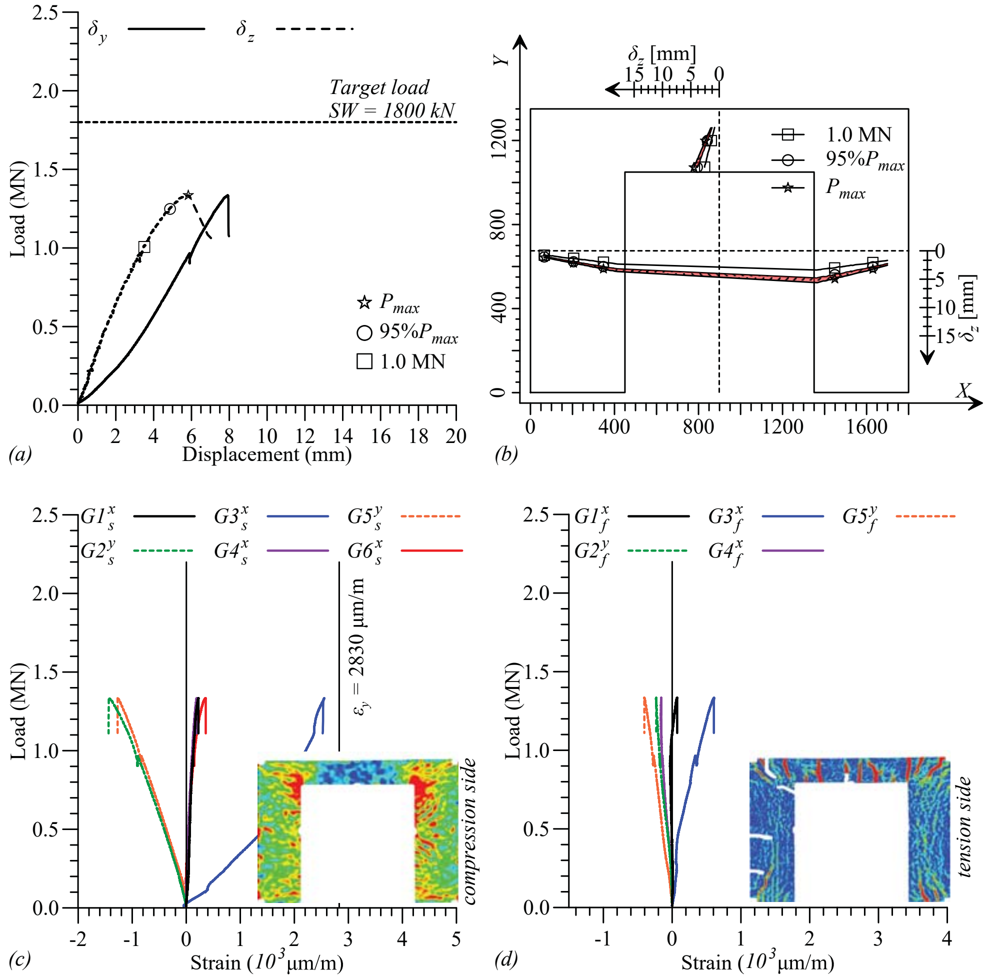

Fig. 9. Response of LO2: (a) load vs. δy and δz; (b) out-of-plane displacement profile; (c) load vs. steel strain and tensile strain

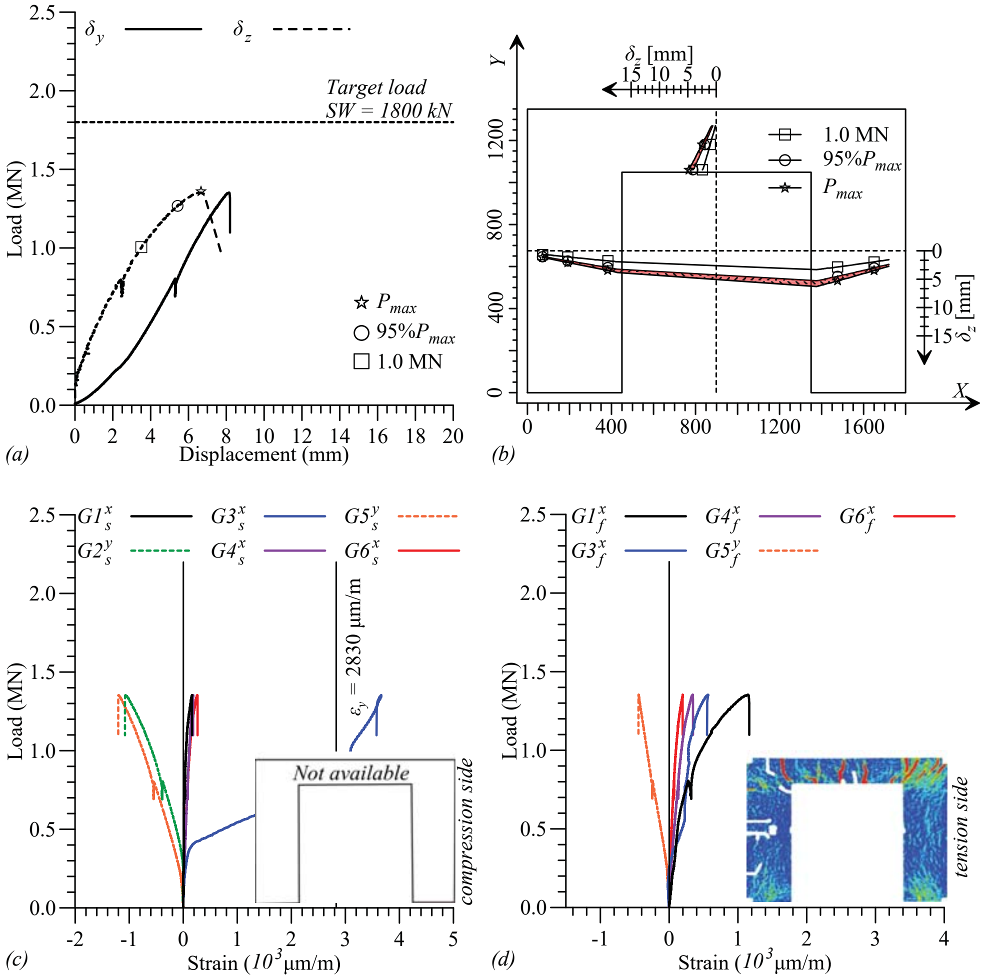

Fig. 10. Failure mode of strengthened panels - concrete crushing at the bottom of the east pier

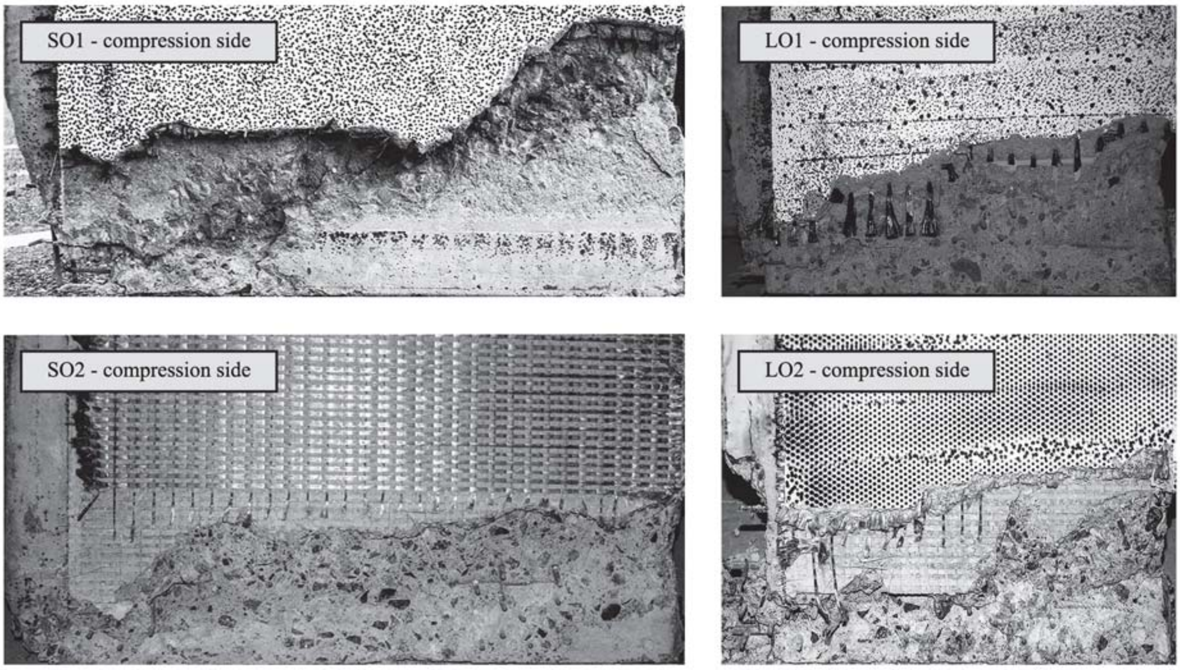

Fig. 11. Load vs. displacement response: (a) out-of-plane displacement ("δ" _"z" ^"D1") and (b) vertical displacement (δy)

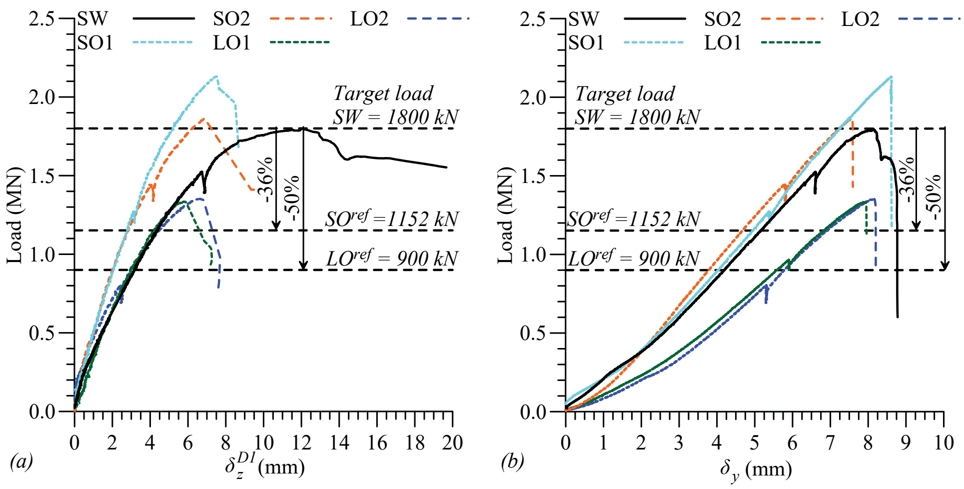

Fig. 12. Geometric properties of SO panel (C - center of gravity
SW; Cx, Cy, centers of gravity of panel with opening in horizontal

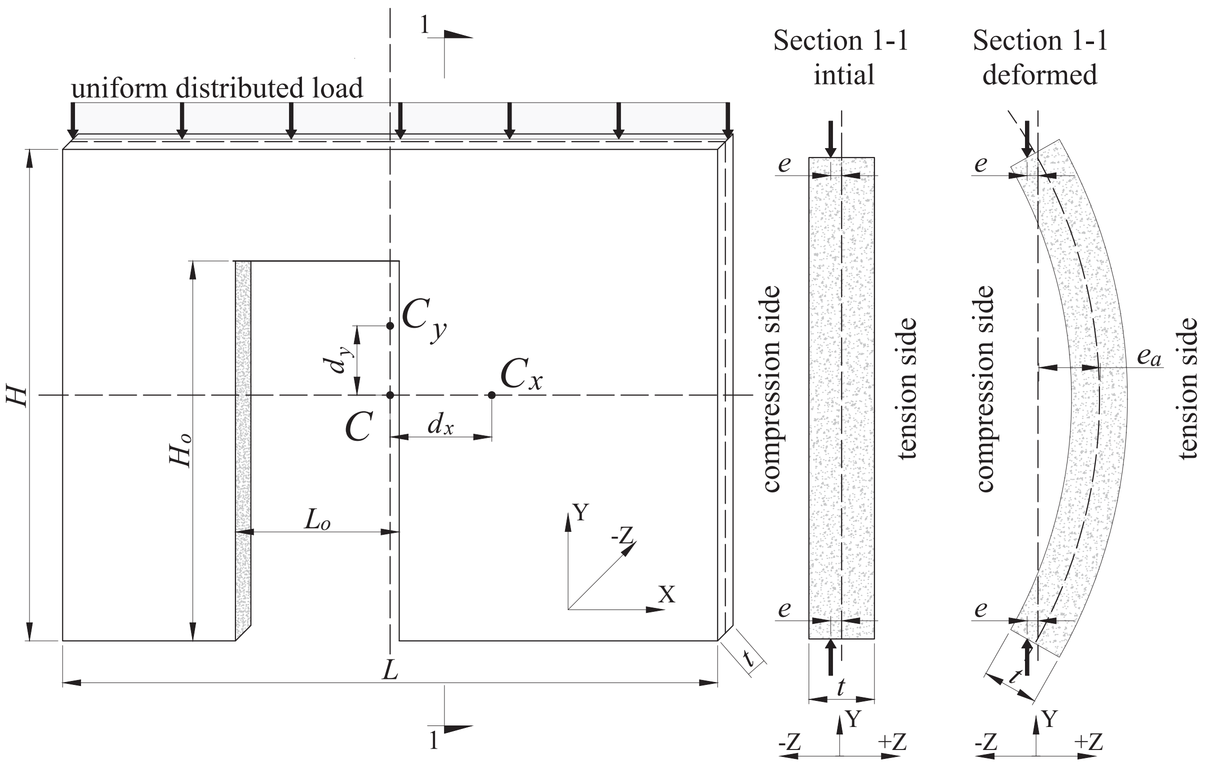

Fig. 1. Geometry, reinforcement and strengthening detail of tested wall panels (dimensions in mm)

Fig. 2. (a) Schematic of ICS setup (dimensions in millimeters); (b) overview of setup - Panel LO1 (color)

Fig. 3. Instrumentation of each specimen type relative to the global coordinate system (color)

Fig. 4. Response of SW: (a) load vs. δ_y and δ_z; (b) out-of-plane displacement profiles; (c) load vs. steel strain and tensile strain distribution, at P_{max}; (d) load vs. concrete strain and compressive-strain distribution, at P_{max} (color)

Fig. 5. Surface strain distribution at maximum and failure loads (color)

Fig. 6. Response of SO1: (a) load vs. δ_y and δ_z; (b) out-of-plane displacement profile; (c) load vs. steel strain and tensile strain distribution, at P_{max}; (d) load vs. fiber strain and tensile strain distribution, at P_{max} (color)

Fig. 7. Response of SO2: (a) load vs. δ_y and δ_z; (b) out-of-plane displacement profile; (c) load vs. steel strain and tensile strain distribution, at P_{max}; (d) load vs. fiber strain and tensile strain distribution, at P_{max} (color)

Fig. 8. Response of LO1: (a) load vs. δ_y and δ_z; (b) out-of-plane displacement profile; (c) load vs. steel strain and tensile strain distribution, at P_{max}; (d) load vs. fiber strain and tensile strain distribution, at P_{max} (color)

Fig. 9. Response of LO2: (a) load vs. δ_y and δ_z; (b) out-of-plane displacement profile; (c) load vs. steel strain and tensile strain distribution, at P_{max}; (d) load vs. fiber strain and tensile strain distribution, at P_{max} (color)

Fig. 10. Failure mode of strengthened panels - concrete crushing at the bottom of the east pier

Fig. 11. Load vs. displacement response: (a) out-of-plane displacement (δ_z^{D1}) and (b) vertical displacement (δ_y) (color)

Fig. 12. Geometric properties of SO panel (C - center of gravity SW; C_x, C_y, centers of gravity of panel with opening in horizontal and vertical planes, respectively) adapted from (Guan et al. 2010)